Astron. Astrophys. 353, 163–176 (2000)

ASTRONOMY AND ASTROPHYSICS

Checking the yellow evolutionary void

Three evolutionary critical Hypergiants: HD 33579, HR 8752 & IRC +10420⋆

H. Nieuwenhuijzen and C. de Jager

SRON Laboratory for Space Research; Sorbonnelaan 2, 3584 CA Utrecht, The Netherlands and Astronomical Institute, Utrecht, The Netherlands

Received 21 December 1998 / Accepted 25 August 1999

Abstract. We have checked the reality of the yellow evolutionary void (which is an area in the Hertzsprung-Russell diagram where atmospheres of blueward evolving super- and hypergiants are moderately unstable), by comparing one star inside the void: HD 33579 (= R76), and two at the low-temperature border of it: HR 8752 (= HD 217476, V509 Cas) and IRC+10420. We found that the first star has a large mass and a fairly stable behaviour over time. These aspects suggest, together with abundance determinations by others, that it is a fairly young, still redward-evolving supergiant. For such a star the void is not forbidden. The two other stars, HR 8752 resp. IRC+10420, have low masses which places them in the post-red blueward loop. They show indications of the expected bouncing effect for blueward returning red supergiants: when approaching the void they eject mass, resulting in a sudden reduction of $T_{\rm eff}$ and a decrease of the atmospheric acceleration to $g_{\rm eff} \simeq$ zero. Thereafter $T_{\rm eff}$ and $g_{\rm eff}$ increase again. For HR 8752 two such recent 'bounces' have been identified. The photometric variations of HR 8752 and of HD 33579 are due to high–l gravity-wave pulsations.

Key words: stars: supergiants – stars: atmospheres – stars: mass-loss – stars: evolution – gravitational waves

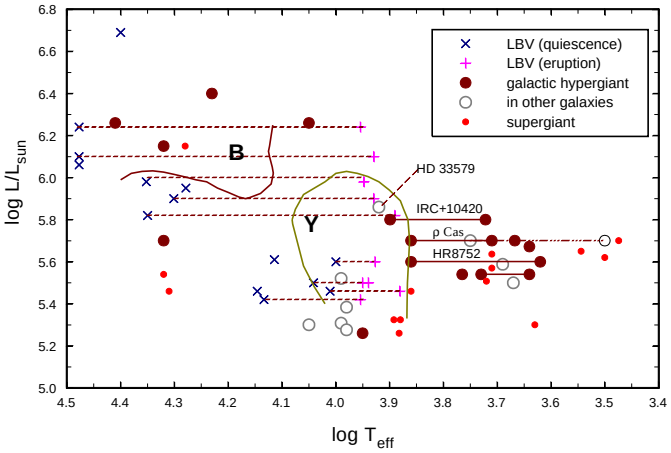

Fig. 1. The HR-diagram for blueward evolution. The diagram shows the yellow evolutionary void (marked **Y**) and the blue instability region (**B**). The diagram is a slight modification of Fig. 1 of de Jager (1998).

1. Checking the yellow evolutionary void

The yellow evolutionary void is an area in the Hertzsprung-Russell diagram, proposed by the present authors (Nieuwenhuijzen & de Jager 1995a). It is the region where for blueward evolving stars (in hydrostatic equilibrium) (1) a negative density gradient occurs, (2) the sum of all accelerations, including wind, turbulence and pulsations, is zero or negative, (3) the sonic point of the stellar wind is reached in or below photospheric levels, and (4) $\Gamma_1 \leq 4/3$ indicating some level of dynamic instability in part of the atmosphere.

Properties of the void and the evolution of ideas about it since 1958 are described in a review paper by de Jager (1998). Fig. 1 shows the upper part of the Hertzsprung-Russell diagram. It applies to blueward evolving stars. The calculated limits of the void and of the 'Blue Instability Region' are drawn. A comparison with supergiants shows that ρ Cas, HR 8752 and IRC+10420, three well-studied yellow hypergiants, are situated at or close to the red border of the void. For these three stars we have plotted in Fig. 1 the range of their $T_{\rm eff}$-values over the last 40 years; cf. also Table 2.

In this paper we want to check observationally the reality of the proposed yellow evolutionary void. We do that by using observations of some selected hypergiants, that are either inside the void (HD 33579), or at the lower temperature boundary of it (HR 8752 and IRC+10420). A fourth interesting star with characteristics similar to HR 8752 is ρ Cas. This is being discussed by Lobel in a series of papers (cf. Lobel et al. 1998).

We compare time histories, using data that span some 10 years or longer, spectroscopic measurements at different times, and evolutionary scenarios from evolutionary calculations. In order to determine the evolutionary status of these stars we are interested to know their spectroscopically derived 'abundances' and also their masses.

We see three or four ways to examine their (in)stability:

Send offprint requests to: H. Nieuwenhuijzen (H.Nieuwenhuijzen@sron.nl)

⋆ Based on observations at the La Palma Observatory and the ESO Observatory in Chili.

a. Position with respect to the void. So far, we know of only three stars that are situated inside the void, HD 33579, HD 7583($\log L/L_\odot = 5.52$; $\log T_{\rm eff} = 3.99$), and HD 168607 (5.60; 4.00–3.93). The latter star is an LBV. The two others are Magellanic Cloud hypergiants. If our assumptions about the void are correct, these stars can only exist in a stable configuration at these places if they are evolving redward. For LBV's the conventional scenario is that they are evolving redward and make redward excursions (Humphreys & Davidson 1979, Humphreys 1989). This may explain why a star like HD 168607 can occur inside the void. For HD 33579 and HD 7583 the question about the evolution can be settled by considering elemental abundances; Humphreys et al. (1997) have shown that HD 33579 has 'normal' abundances which suggests redward evolution. For HD 7583 we do not possess such spectroscopic data.

b. Mass. Another way is to compare the mass expected from evolutionary calculations with the value derived from spectral observations. That is done in this paper for HD 33579, HR 8752 and IRC+10420. For the former one should expect a mass closer to the ZAMS value while the yellow hypergiants HR 8752 and IRC+10420 should have relatively small masses, in accordance with their expected evolutionary status.

In Sect. 4 we describe a technique for obtaining the values of the masses from spectroscopic data.

c. Emission of gas shells. When a star, in its blueward (returning) evolution, approaches the void its increasing instability might show itself by the emission of gas shells. A possible scenario may then be that the star 'bounces' several times to the low-temperature border of the void, thereby losing mass each time. That should then be a property of HR 8752 and IRC+10420, but not of HD 33579. The star IRC +10420 is indeed known to have developed an extensive obscuring gaseous and dusty envelope.These aspects are dealt with in Sect. 3.

d. Pulsational motions. A possible fourth way might be to study atmospheric pulsational motions for the three stars (Sects. 5, 6 and 7). We will present indications suggesting their relation to the photospheric instability.

2. Spectroscopic determination of the atmospheric parameters

2.1. Method

The basis of our method of analysis has been described earlier (Achmad et al. 1991b, Lobel et al. 1992) and consists of assuming starting values for four photospheric parameters, the first two being (1) $T_{\rm eff}$ and (2) $g_{\rm K}$, the Kurucz model parameter. That latter parameter is not neccessarily equal to the Newtonian value $g_{\rm N}$, nor is it equal to the effective acceleration $g_{\rm eff}$. For that reason we call it $g_{\rm K}$, to distinguish it clearly from other g-parameters. Actually

$$g_{\rm eff} = g_{\rm K} + g_{\rm rad}$$

($g_{\rm rad}$ is directed outward, hence has a negative sign). The third and fourth photospheric parameters are (3) $\zeta_{\rm t}$, the line of sight component of the small-scale motions ('microturbulence'), and (4) $[Z/H]$, the log of the relative metal abundance relative to that for the Sun. For a given range of photospheric Kurucz models based on variations in these four parameters, equivalent widths (W) are computed for a set of observed lines. A least-squares comparison of the observed equivalent widths $W_{\rm obs}$ (cf. Tables A2 to A5) with the calculated model values of the equivalent widths yields a vector in four-dimensional space, that gives a 'better' set of values for the four photospheric parameters in the least-squares or minimum-χ^2 sense. In several subsequent approximations one thus arrives at the 'best' values. The found values are numerically interpolated from the available Kurucz models, discrete in $T_{\rm eff}$, $\log g_{\rm K}$. For the extreme stars that we research here, it may happen that the found values for $\log g_{\rm K}$ lie outside the given model ranges. In these cases the indicated best-fit values for $\log g_{\rm K}$ have meaning only if they indicate atmospheres with parameter values that are not far from existing models (extrapolation).

We have sharpened the above basis by trying to obtain an unbiased estimate of the atmospheric parameters by taking into account derived tolerances in the observed equivalent widths of the lines, and tolerances in the accuracies of the comparison data (the atomic gf-values). We have tested this concept in the following analyses. We estimate the influence of the chosen continuum level on the equivalent width by fitting gaussian line profiles. For the gf-values we use the data from Martin et al. (1988), who give accuracy classification for the lines they have compiled, which we use as indicated below. For data not in their lists, we have used the gf-values of Kurucz & Peytremann (1975).

Also, different lines are not equally sensitive to variations of the photospheric parameters; obviously lines on the flat part of the curve-of-growth are insensitive. These effects have to be included in the line-model computations that we use as reference.

For the sets of data from earlier authors we used the same method as above, assuming an estimated uncertainty of the measured equivalent width of 10%.

2.2. Computational method

We define $\sigma_{\rm obs}$ as the r.m.s. tolerance in the observational equivalent widths, found from a comparison of various determinations of the observed equivalent width $W_{\rm obs}$ after having added an estimated contribution of the errors due to the uncertainty in the continuum level. Further, we define $\sigma_{\rm cal}$ as

$$\sigma_{\rm cal} = \frac{\partial W}{\partial \ln gf} \times \Delta \ln gf. \qquad (1)$$

Here, W is the equivalent width value calculated for a line (for a given model), and $\Delta \ln gf$ is the estimated accuracy in the values of gf as given in the tables of Martin et al. (1988). Table A1 (in the Appendix) lists the adopted numerical values for the various letter codes used (loc. cit.).

In practice the partial differential is computed for the nominal gf-value and one that is 10% higher for each line. This

Table 1. Photospheric parameters derived for for the three stars, data from indicated sources

$*$	date yr/mo	$T_{\rm eff}$ K	$\log g_{\rm K}$ $\rm cms^{-2}$	$\zeta_{\rm t}$ $\rm kms^{-1}$	$\log Z/H$	Reference
HR 8752	1973/08	4930 ± 40	-1.8 ± 0.3	5.3 ± 0.2	-0.1 ± 0.06	reanalysis Luck (1975)
	1978/08	5540 ± 170	0.15 ± 0.44	11.6 ± 0.8	0.1 ± 0.11	Victoria B.C. data, this paper
	1984/07	4570 ± 400	$-6? \pm 1.5?$	4.9 ± 0.4	0.1 ± 0.4	reanalysis Piters et al. (1988)
	1995/04	7170 ± 340	-0.18 ± 0.5	13.2 ± 0.5	-0.25 ± 0.05	La Palma data, this paper
HD 33579	1986/12	7980 ± 160	0.82 ± 0.21	10.5 ± 0.5	-0.38 ± 0.14	Groth, private communication
IRC +10420	1994/07	7930 ± 140	0.01 ± 0.28	10.1 ± 0.3	-0.18 ± 0.12	Oudmaijer (1995), this paper

is done for each photospheric model separately and the results are stored with the model parameters to allow the minimum-χ^2 procedure to work with discrete models.

The calulated χ^2 is then derived according to

$$\chi^2 = \frac{\sum (W_{\rm obs} - W_{\rm cal})^2}{\sigma^2_{\rm obs} + \sigma^2_{\rm cal}} \qquad (2)$$

It is used for determining the mean errors of the four model parameters.

The results of the spectral analyses are summarized in Table 1. Some reference data for the spectra that we have used are also listed in Table 1.

Noteworthy is the considerable change in $T_{\rm eff}$ of HR 8752 during the considered period (cf. Table 2). In a period of only 10 years the temperature fluctuated over a range of more than 2000 degrees. We discuss the time variation of $T_{\rm eff}$ in some more depth in Sect. 3. The same applies to IRC+10420 (Oudmaijer 1995; Klochkova et al. 1997) of which only one datum point is given here.

2.3. Procedure

The procedure is as follows. We use Kurucz models (Kurucz 1979) for the LTE, plane parallel atmospheres, and a code 'Scan', developed from a code initially produced at Kiel (Baschek et al. 1966), adapted by Burger (1976), further modified by P. Mulder in 1983, by P. van Hoof, rewritten by C. de Jager, H. Nieuwenhuijzen and L. Achmad in 1990 (unpublished), to find the integrated line intensities ('equivalent widths') of selected lines. We use this code to generate a list of equivalent widths for a grid of models for two different values of microturbulence.

3. Long-term variability

It is interesting to compare the time histories of these stars. One star seems stable in time, while the others show significant changes. A discussion of known data of the stars follows below.

3.1. A time-line for HR 8752

The properties of this star with its interesting recent life history were described by various authors, among which Lambert & Luck (1978), de Jager (1980) (summary on p. 102f), Zsoldos (1986a, 1986b), Sheffer & Lambert (1987), Piters et al. (1988), Percy & Zsoldos (1992) and de Jager & Nieuwenhuijzen (1997). The most noteworthy properties of the star are its gradual change of the V-magnitude from $\simeq 5.8$ in 1850 till $\simeq 5.0$ in 1970 (Zsoldos 1986a), and the rapid changes in spectral type and colour over the past fifty years (Lambert & Luck 1978). Assuming that the bolometric luminosity did not change in the last century, the first observation means that $M_{\rm bol} - V$ changed by about one magnitude, which implies *a gradual increase of $T_{\rm eff}$ by about 1000 K in 100 years*.

We summarize in Table 2 recent data on spectral type and $B-V$-values found in literature (references in the last column of the Table) for HR 8752.

Table 2. The variation of spectral type, $B-V$-values and $T_{\rm eff}$ for HR 8752 over the last half century, as collected from literature, to which we have added the $T_{\rm eff}$-values derived in this paper. When only the year of publication is known and not that of the observation, an asterisk (*) is added to the year in the first column. A reanalysis of data from Luck (1975) and from Piters et al. (1988) is indicated by an asterisk (*) after the name in the Reference column. Patterson (1990) gives spectral class G4v0 and $T_{\rm eff} < 5500\,K$; we estimate the temperature from the spectral classification G4Ia as indicated here below. To facilitate a comparison of the date we have transformed spectral types or $B-V$-values into $T_{\rm eff}$- values by using the conversion tables of de Jager & Nieuwenhuijzen (1987)

yr/mo	Spectr.	$B-V$	$T_{\rm eff}$	Reference
1950/9	G3Ia	-	4820	Keenan (1971)
1953*	-	1.29	4300	Johnson & Morgan (1953)
1957/9	G0Ia	-	4940	Keenan (1971)
1961	G0Ia	-	4940	Sargent (1965)
1961*	-	1.46	4010	Kraft & Hiltner (1961)
1963*	-	1.39	4130	Oja (1963)
1963*	-	1.38	4150	Sandage & Smith (1963)
1965*	-	1.55	3790	Iriarte & Johnson (1965)
1970/10	G4Ia	-	4630	Keenan (1971)
1970/11	-	-	5000	Fry & Aller (1975)
1973	K2-5Ia	-	4250	Luck (1975)
1973/8	-	-	4930	Luck (1975) *
1974	G4Ia	-	4630	Morgan et al. (1981)
1976	G5Ia	-	4900	Sheffer & Lambert (1992)
1978/8	-	-	5540	Victoria B.C. data, this paper
1980/8	G4Ia	-	5190	Patterson (1990)
1984/7	-	-	4570	Piters et al. (1988) *
1991	F8Ia	-	6150	Sheffer & Lambert (1992)
1995/4	-	-	7170	La Palma data, this paper

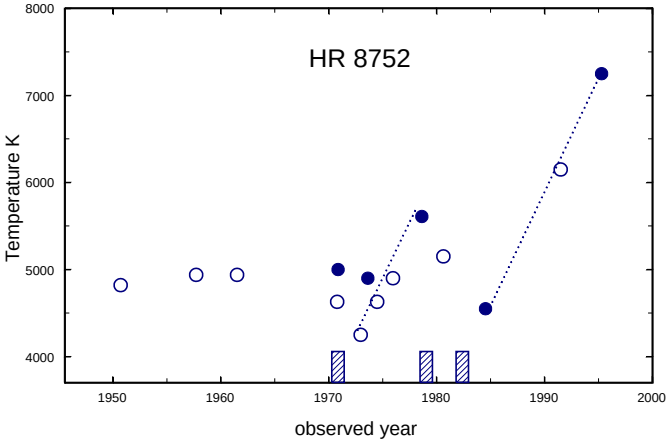

Fig. 2. Variation of $T_{\rm eff}$ of HR 8752 between 1950 and present. *Open circles*: Effective temperatures derived from $B-V$ values; *Filled circles*: Values derived from spectral analysis.

The $T_{\rm eff}$-values of Table 2 are plotted in Fig. 2 as a function of time. We did not include the values for which the date of observation is uncertain. The $T_{\rm eff}$-data can be related to periods of observed enhanced mass loss. Smolinski et al. (1989) mention three periods of enhanced mass ejections, these being the years 1970, 1979 and 1982. We have marked these periods by small boxes with hatching along the time axis. As a next step we have tentatively drawn the dotted lines through the $T_{\rm eff}$-points. These lines may suggest the 'bouncing effect' mentioned earlier: when the star has obtained a high $T_{\rm eff}$ while approaching the low-temperature border of the void, excessive mass is ejected and the (resulting) optically thick shell then causes $T_{\rm eff}$ to decrease. When the ejected shell gradually becomes transparent, $T_{\rm eff}$ increases again. These conclusions are not in disagreement with those of Lambert et al. (1981) who studied the circumstellar CO-lines of this star. P Cygni profiles appeared in 1976 changed a few years later to inverse P Cygni profiles indicated a back-falling shell, with in 1979 an infall rate of $\approx 30 {\rm kms}^{-1}$.

Fig. 2 also suggests that a next shell ejection may be imminent; never before has $T_{\rm eff}$ been as high as in 1995. Frequent spectral and photometric observations of this star are certainly rewarding.

3.2. HD 33579

The star HD 33579, spectral type A3Ia$^+$, situated in the Large Magellanic Cloud is one of the most luminous yellow stars known outside our Galaxy. Because of its spectral type we call it a white hypergiant, in contrast to the yellow and red ones, which constitute the main body of the hypergiants. In the literature there is no indication of any significant variation of spectral type or effective temperature with time. Its main parameters for the period 1968–78 were summarized by de Jager (1980; Table XX, p. 105), from a compilation of data from Wolf (1972), Wares et al. (1968), Przybylski (1968), Walraven & Walraven (1971), and van Genderen (1979a). They were $T_{\rm eff}$ = 8130 $\pm$ 300 K, log$g$ = 0.7 $\pm$ 0.2. About 15 years later the effective temperature was still 7980 $\pm$ 160 and $\log g_{\rm K}$ = 0.82 $\pm$ 0.21, as shown in Table 4. This is no significant change as compared with the earlier period, which is in sharp contrast to the strong variability observed in HR 8752. From a non-LTE atmospheric model study Groth et al. (1992) derived for HD33579 $T_{\rm eff} = 8500\,K$ and $\log g = 0.85$. HD 33579 shows a constant behaviour during the same observational period as described for HR 8752; it shows no evidence of a "bounce".

3.3. IRC+10420

In a study on the spectral energy distribution of IRC+10420 Oudmaijer et al. (1996) have determined the best fitting Kurucz models to the photometry for observations in 1974 and 1992 respectively. They discuss that the observed changes can reflect a change in stellar temperature while the bolometric luminosity and the extinction (circumstellar and interstellar) remain the same. The temperature could then have increased from 6000 K in 1974 to $\simeq$ 7000–7500 K in 1992. From high resolution spectra Oudmaijer (1998) concludes that the spectral changes are an independent confirmation of the interpretation of the increase in temperature over the last 20 years.

Our reanalysis of Oudmaijers 1994 spectral data (Oudmaijer 1995, 1998) gives a value of 7930 $\pm$ 140 K, which is in not unreasonable agreement with the findings of Oudmaijer (1998), who states that the spectral type of IRC +10420 has changed from F8 in 1973 to A-type in 1994, which implies that the temperature of IRC +10420 has increased by 1000–2000 K (thus resulting in 7000–8000 K).

Using optical spectra obtained with the 6-m telescope of the Special Astrophysical Observatory, Russian Academy of Sciences, from 1992 to 1996, together with the data from Oudmaijer, (loc. cit.), Klochkova et al. (1997) estimate the atmospheric parameters as $T_{\rm eff}$ = 8500 K, $\log g$ = 1.0, $\zeta_{\rm t}$ = 12 km s^{-1}, and an average value for the metallicity of -0.03. Classifying IRC+10420 as presently having a spectral class of A5, a type that should be compared with the earlier allocated spectral type of F8-G0 I (Humphreys et al. 1973), they conclude that the star has a rise in temperature of some 3000 K in about 20–22 years, and that "a combination of results allow" them "to consider IRC+10420 as a massive supergiant evolving to the WR stage." This conclusion is amplified by the observed expanding shell of gas and dust around the star (summarized in de Jager 1998, pp 156–157 and described in detail by Humphreys et al. 1997).

The existence of a large gas/dust shell around that star would indicate that a severe mass-loss period occured perhaps 200 years ago (estimate in Oudmaijer 1995 (p. 183) and in Oudmaijer et al. 1996 (Sect. 5.1)). IRC+10420 might follow a warming-up similar to HR 8752 before a "bounce".

3.4. Conclusions

We find that the temperature variations of HR 8752 showed a repetitive process that we call 'bouncing against the low–T boundary of the void'. Since 1985 its $T_{\rm eff}$- value has increased by

nearly 3000 K. Also IRC +10420 has increased its temperature, by some 3000 K in about 20 years. Fairly recent enhanced mass loss is suggested by its shell. In contrast HD 33579 is remarkably stable and quiet.

4. Determining spectroscopic masses

4.1. Deriving masses from the gradient of $P_{\rm g}$

Since the stars are not close binaries, spectroscopic methods have to be used.

To determine stellar masses we use a method as given in an earlier paper (Nieuwenhuijzen & de Jager 1995b). It is partly based on our improved technique to find best-fit model data of atmospheric parameters from observed spectral line equivalent-widths, described in Sect. 2. The gradient of the gas pressure at a distance r to the stellar centre can be written as

$$-\frac{dP_{\rm g}}{dr}=\rho g_{\rm N}(1-\Gamma)\left(\frac{R}{r}\right)^2+\frac{\rho}{2}\frac{dv_{\rm w}^2}{dr}+f_{\rm turb} \qquad (3)$$

where R is the 'radius' of the star, Γ the Eddington parameter to include the effect of radiation pressure, $v_{\rm w}$ the local stellar wind velocity, and $f_{\rm turb}$ the turbulence term. Application of this expression implies knowledge of the rate of mass loss $\dot{M}$, for calculating $v_{\rm w}$.

The turbulent contribution is

$$f_{\rm turb}=\frac{dP_{\rm turb}}{dr}=\frac{1}{2}\frac{d\rho\zeta_{\rm t}^2}{dr}\ , \qquad (4)$$

and since in stars of these types $\zeta_{\rm t}$ is practically independent of height (Achmad et al. 1991a; Lobel et al. 1992)

$$f_{\rm turb}=\frac{1}{2}\zeta_{\rm t}^2\frac{d\rho}{dr}\ . \qquad (5)$$

We stress here that $\zeta_{\rm t}$ is not a 'fudge factor' as is sometimes claimed. It represents real physical motions (Smith & Howard 1998), probably a field of shock waves (de Jager et al. 1997). If the gravitational acceleration component $g_{\rm N}(R)$ is known from Eq. (3), then

$$g_{\rm N}(R)=-\frac{GM(R)}{R^2}\ ,$$

where R is derived from L and $T_{\rm eff}$. Hence we need to know $g_{\rm K}$, $T_{\rm eff}$,$\zeta_{\rm t}$, L, $\dot{M}$ and the density gradient to derive the mass M. The first three data are derived in Sect. 2.

4.2. Determining L and $\dot{M}$

For the luminosity of HD 33579 we refer to Wolf (1972). The distance modulus as found from combining data of Hipparcos by Walker (1999) is 18.55 $\pm$0.10, which value does not hardly differ from the value of 18.5 as given by Tifft & Snel (1971), which value was used by Wolf (1972). For the luminosities of HR 8752 and IRC+10420 we used the compilation by de Jager (1998).

The rates of mass loss are for HD 33579 $\log\dot{M}$ = -5.7 (Stahl et al. 1991) and for HR 8752: -4.92 (de Jager et al. 1988). However, because the stars will have a varying amount of mass loss in their time-histories, we have taken a mean value, for which we choose, admittedly arbitrarily, $\log\dot{M}$ = -4.7. It turns out that the contribution of the $\dot{M}$-term for HD 33579 is practically negligible, and hence the results for this star are not influenced by this decision; in the final calculations we used the value given by Stahl et al. (1991). In seperate calculations we varied the massloss by a factor of two upwards, which in all cases, except for IRC+10420 resulted in practically negligible changes in the derived masses.

4.3. Mass determinations

The required values of $g_{\rm K}$, $T_{\rm eff}$ and $\zeta_{\rm t}$ are given in Table 1, while Table 4 gives the commonly adopted values of $\log L/L_\odot$ and $\dot{M}$ for the three stars (cf. Sect. 4.2).

We rewrite Eq. (3) as

$$-\frac{1}{\rho}\frac{dP_{\rm g}}{dr}\equiv g_{\rm eff}=g_{\rm N}(1-\Gamma)\left(\frac{R}{r}\right)^2+\frac{1}{2}\frac{dv_{\rm w}^2}{dr}+\frac{1}{2}\zeta_{\rm t}^2\frac{d\ln\rho}{dr} \qquad (6)$$

With $g_{\rm eff}=g_{\rm K}+g_{\rm rad}$ (cf. Sect. 2.1) one obtains

$$g_{\rm K}=g_{\rm N}\left(\frac{R}{r}\right)^2+\frac{1}{2}\frac{dv_{\rm w}^2}{dr}+\frac{1}{2}\zeta_{\rm t}^2\frac{d\ln\rho}{dr}\ . \qquad (7)$$

We applied this equation to the photospheric level $\tau_{\rm R}=0.03$ since that is the average level of line formation (Achmad et al. 1991a; Lobel et al. 1992). By interpolating (or slightly extrapolating) Kurucz models to the $T_{\rm eff}$ and $g_{\rm K}$ values of Table 1 we derived for the level $\tau_{\rm R}=0.03$ values of $d\ln\rho/dr$.

Since $r=R=\left(L/(4\pi\sigma T_{\rm eff}^4)\right)^{1/2}$, at the level where $T(\tau)=T_{\rm eff}$ we also read from the inter/extra-polated model the value $r(\tau=0.03)-R$ for this model. Finally, for that depth level

$$v_{\rm w}=\dot{M}/4\pi r^2\rho\ . \qquad (8)$$

Thus $g_{\rm N}$ is found and hence the stellar mass, which we present in Table 4, expressed in solar units.

We note here that the value of $g_{\rm N}$ depends on the value of $g_{\rm K}$ through the use of the various other terms in Eq. (7), for the $\tau_{\rm R}$-value at which the lines originate. Through the χ^2-minimization process we find an atmosphere with a $g_{\rm K}$-value that best fits the line data at some mean τ-value of line origination. This value we take to be $\tau_{\rm R}$=0.03.

In Table 3 we show the influence of the choice of the representative layer for finding the effective and Newtonian accelerations for one and the same $g_{\rm K}$ and for different $\tau_{\rm R}$-values for HD 33579, using our models as explained here and in Nieuwenhuijzen & de Jager (1995b).

The table clearly shows an effect that is nearly always neglected in studies of stellar mass determinations: it is absolutely necessary to know the level of line formation for deriving a reliable mass value.

It explains at the same time the reason why our mass determination differs from former ones (cf. Wolf 1972), where the reference data applies to the photospheric level around $\tau=2/3$ or perhaps $\tau=0.3$ (where the used microturbulent velocity in Wolf's (1972) Table 5 is 10 km s^{-1}).

Table 3. The importance of choosing a correct representative value of $\tau_{\rm R}$ on the mass of the star HD 33579 is illustrated by models with varying mass and further identical stellar parameters as given in Tables 2 and 4, with $\log g_{\rm K}$=0.82 for each given $\tau_{\rm R}$-value. M is given in solar masses.

HD 33579							
$\tau_{\rm R}$	$\log g_{\rm r}$	$\log g_{\rm w}$	$\log g_{\rm t}$	$\log g_{\rm e}$	$\log g_{\rm N}$	$\log M$	M
0.666	0.645	-5.350	-0.131	0.341	0.864	1.576	37.7
0.300	0.447	-6.657	0.946	0.580	0.756	1.468	29.4
0.100	-0.006	-5.881	0.612	0.750	0.923	1.638	43.5
0.030	-0.238	-4.229	0.809	0.780	1.107	1.823	66.5
0.010	-0.315	-3.319	0.840	0.787	1.131	1.849	70.6

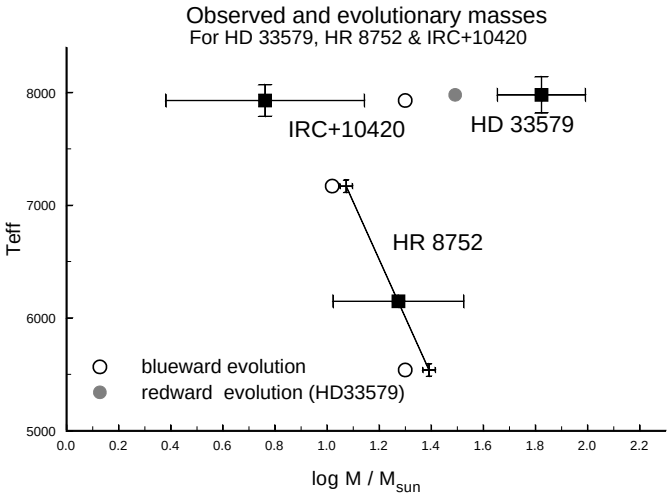

Fig. 3. Observationally derived values of $T_{\rm eff}$ and $M/M_{\odot}$ for HD 33579, HR 8752 and IRC +10420. Black squares are observations, circles are masses according to evolutionary calculations. For HR 8752 the crosses refer to the mass determinations in 1978 (lower T) and 1995. The filled square with the error box is the average mass. The circles are (T, M)-values that would be derived from evolutionary calculations if the star's temperatures would be related to their evolution (which is not the case for HR 8752), therefore use of an average temperature is a better representation.

4.4. The dependency of $M(L, T_{\rm eff})$ on L, $T_{\rm eff}$ and $g_{\rm N}$

Being given the uncertainties in the the basic data ($T_{\rm eff}$, $g_{\rm K}$, L, $\dot{M}$, $\zeta_{\rm t}$) the resulting $g_{\rm N}$ and mass M are uncertain too. The dependency of the mass on the assumed values of $T_{\rm eff}$ and L can be read from

$$M = g_{\rm N}\frac{R^2}{G} = g_{\rm N}\frac{1}{G}\frac{L}{4\pi\sigma T_{\rm eff}^4},$$

a form that applies to the level where $T = T_{\rm eff}$. For a grey atmosphere $T = T_{\rm eff}$ at $\tau = 2/3$. For non-grey atmospheres this τ-value may differ slightly from 2/3.

5. Comparison with evolutionary masses

5.1. Masses from evolutionary models

In order to decide in which part of the evolutionary scenario a star can be actually be situated, we compare the observed actual mass with that of evolutionary calculations (Maeder & Meynet 1987, 1988) by way of a computer program as mentioned in Nieuwenhuijzen & de Jager (1990). This program determines the mass as a function of the position of the star in the HR-diagram for a selected 'track', here: redward or blueward evolution. For our stars the values thus expected are given in the last two columns of Table 4. The expected positions of HR 8752 and IRC +10420 are given by open circles in Fig. 3.

5.2. The observational mass for HD 33579

For a Rosseland τ- value of 0.03 we obtain for the 0.68 significance (1σ) level values of $\log M = 1.823(\pm 0.17)$ or a mass value of 67 (+32; -21) solar masses.

For a star with the luminosity of HD 33579, Maeder & Meynet (1987, 1988) predict masses of 35 and 20 $M_{\odot}$, depending on whether the star is evolving redward or blueward, respectively. Both values are much smaller than ours, and the former differs (in logarithm units) by $2\,\sigma$ from the observational one. The second value differs still more and is definitely too low. While being surprised by the high observational mass value, we tend to *conclude* that the high observational mass value is the best one, and that the star must still be evolving redward. This conclusion is consistent with Humphreys et al.'s (1991) finding that the abundances are 'normal', which implies redward evolution, and with the fact that van Genderen (1979a, 1979b) found the star to be photometrically rather stable (cf. Sect. 6). These results somewhat support our ideas on the yellow evolutionary void. We expect that blueward evolving stars, hence objects in their late evolution, if placed at the position of HD 33579, would not or hardly exist, because their evolution goes too quickly, but a redward evolving star can exist at that position.

5.3. The derived mass for HR 8752

Along the same line as for HD 33579 we find the following:

From the observations of HR 8752 in 1973 and 1984 it appears that the effective accelerations are effectively zero (cf. Table 1). Since photospheric models are lacking for such values, we are not able to deduce a mass from these observations.

From the 1995 resp. 1978 measurements we find with 68% significance two different values for the mass (in logaritmic units): 1.07 ± 0.41 resp. 1.39 ± 0.32. Combining the two observations this leads to a mean logarithmic value of 1.27 ± 0.25, which corresponds to a mass of 18.8 (+14.7; -8.2) solar masses. The mass values are given by the oblique cross in Fig. 3, where the filled square gives the average value. It appears that the observational mass is in fair agreement with results of evolutionary calculations (blueward). We think therefore, that with respect to luminosity, $T_{\rm eff}$ and mass, the observations of HR 8752 in 1978 and 1995 seem to follow this evolutionary scenario.

Table 4. Basic stellar data, and masses in solar units (logarithmic) for the three stars, together with the results from evolutionary calculations, interpolated from Maeder & Meynet (1987, 1988), different for redward- and blueward evolution. The observed mass-values are interpreted to be valid for lines originating at a τ-level of 0.03.

star	year	$\log L/L_\odot$	$\dot{M}$	$\log M$		$\log M(red)$	$\log M(blue)$
HR 8752	1973	5.6	-4.7	- - -			
HR 8752	1978	5.6	-4.7	1.391	± 0.315		
HR 8752	1984	5.6	-4.7	- - -			
HR 8752	1995	5.6	-4.7	1.073	± 0.414		
HR 8752	mean	5.6	-4.7	1.274	± 0.251	1.45	1.30–1.02
HD 33579	1986	5.72	-5.7	1.823	± 0.169	1.49	1.30
IRC +10420	1994	5.8	-4.7	0.762	± 0.381	1.55	1.3

5.4. The derived mass for IRC+10420

For IRC+10420 we find with 68% significance a logarithmic mass of 0.76 $\pm$ 0.38, leading to a mass of 5.8 (+8.1; -3.4) in solar units. In his thesis Oudmaijer (1995, p. 180) gives an estimate of the mass of the dustshell of about 40 solar masses if the star is located at a distance of 3.5 kpc. Assuming a ZAMS mass of 50 solar masses, this would lead to an actual mass of some 10 solar masses, in reasonable agreement with our result. Evolutionary calculations, though, predict a larger mass, as appears from the open circle for blueward evolution in Fig. 3. Our result suggests that the star must have lost more mass than is assumed in evolutionary calculations. Hence the excessive mass loss and shells of IRC +10420 still present a problem.

5.5. Conclusion

Observationally derived mass-values are regrettably uncertain but an acceptable conclusion is that the masses confirm that HD 33579 ($67M_\odot$) is evolving redward, and that HR 8752 ($19M_\odot$) and IRC +10420 ($6M_\odot$) are evolving blueward, as we would expect from their positions relative to the void.

6. Short-term photometric observations

The photometric data from HIPPARCOS offer a fine coherent set of observations that can be used for studying periodicities in the variation of stellar luminosity. They are used to investigate the characteristics of the stellar photospheric pulsations.

For HD 33579 and HR 8752 HIPPARCOS data are available; IRC +10420 was too weak for HIPPARCOS. For the first star van Genderen (1979a, 1979b) published photometric data over a time interval of $\approx$ 2800 d (JD 2441800–2444600). For the period JD 2443500-2444585 Grieve & Madore (1986a,b) published some photometric observations of HD 33579 (= S67-44). A combination of these data covers a time span of about 20 years. The photometric data were reduced to the same magnitude scale by using the zero-point difference $V - HP_{\rm dc}$, where $HP_{\rm dc}$ are the Hipparcos magnitudes, as given by van Leeuwen et al. (1998) and shown in Fig. 4 (upper left panel).

For the two stars we derived Lomb normalized periodograms (cf. Press et al. 1992). As an example Figs. 4a, b, c and d give the for HD 33579 the full set of photometric data, the HIPPARCOS data, the $P(\nu)$ and the $P(p)$ diagrams, where P is the power, ν the frequency (d^{-1}) and p the period d. In these diagrams horizontal lines give the probabilities that the data are chance data. The significance levels were estimated using the number of measurement points as the number of 'independent' frequencies. We checked by independent calculations that the upper envelope for the combined ('total') data set is situated at $P = 4$ to 5 for $p \approx 30$ d, smoothly decreasing to $P = 2$ to 3 for $p \approx 600$ d. Hence it is situated well below the level of 50% chance. The multiple splitting of components, apparent in the lower left panel (for the combined data) has no stellar origin but is due to the blank spaces in the data set. In the discussion of the data we have decided to exclude periodogram data below $p \approx 20$ d, which is a period about twice the average spacing in the data from HIPPARCOS and van Genderen (1979a, 1979b). We also decided to only use periods $<$ one-half the period of HIPPARCOS observations because periods outside this interval may be contaminated by noise and may not reliable. We only used data for which the chance probability is smaller than 0.1. We next go to a detailed description of the observations.

6.1. HD 33579

Van Genderen (1979a, 1979b) found that the lightcurve is fairly regular, with only a periodicity of around 100 d. The HIPPARCOS photometric observations, obtained through the intermediary of Dr. van Genderen, are shown with their error-bars in the 2nd panel of Fig. 4. Restricting our analysis to the range of periods $20 < p < 600$ d (as described above), and to periods for which the probability that they are due to chance is < 0.1, we find four components around van Genderen's (1979a, 1979b) period of ≈ 100 days. A remarkable feature is that the number of components, their power (and hence their significance) and even their frequencies seem to change with time. To show this we have split the material in four time-interval groups, as in Table 5.

The frequency variations seem to be real. The highest values for the frequencies appear to occur in the second and third period of van Genderen's (1979a, 1979b) observations. Tentatively we assume the frequency variations to be due to density variations in the atmosphere, assuming the frequency ν to be proportional to $\rho^{\frac{1}{2}}$. To investigate the aspects of this assumption we took

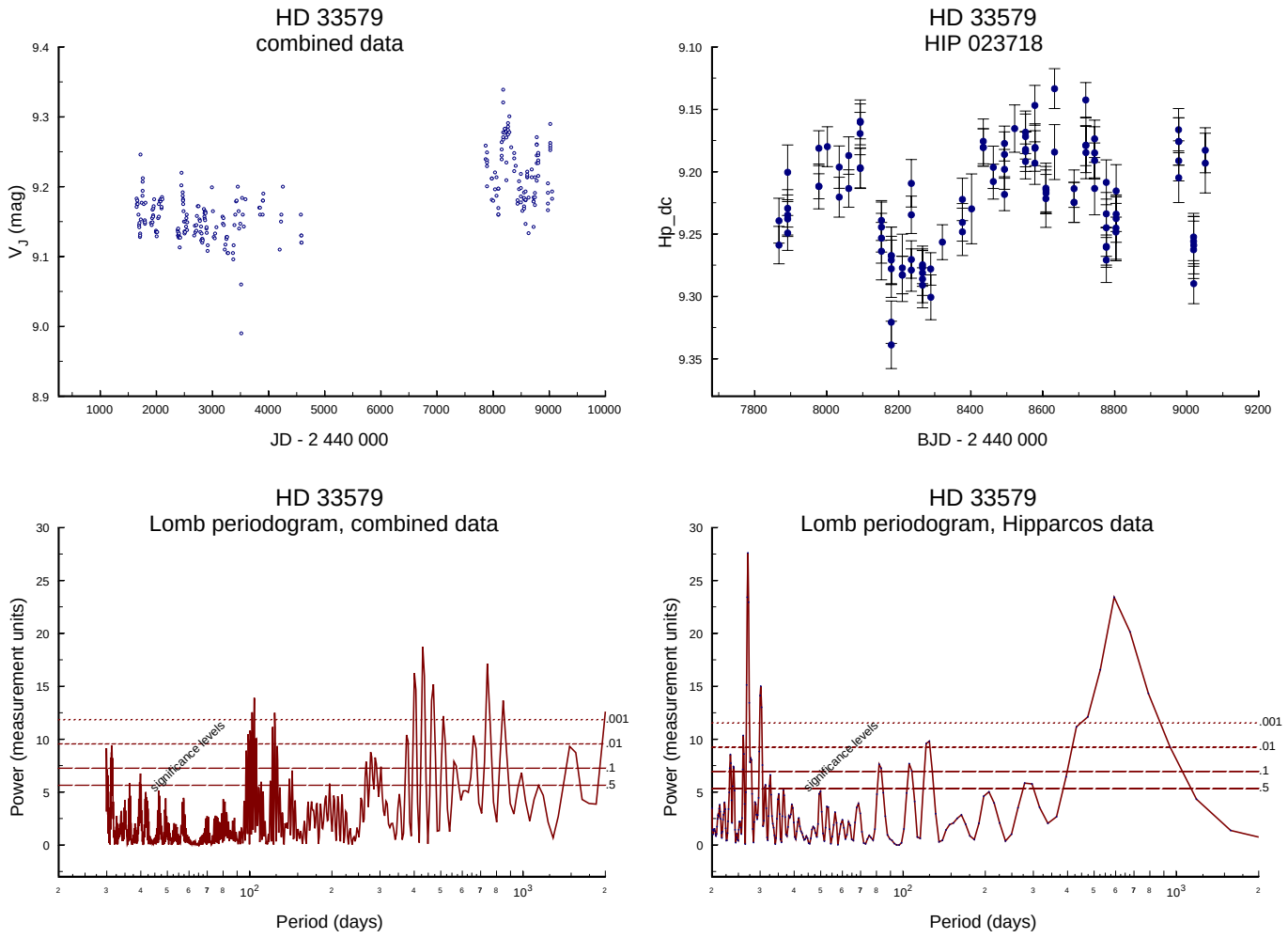

Fig. 4. Light variation of HD 33579. The Lomb normalized periodogram shows the periods of the variations and their intensity. The upper two panels show: the photometric data; *left*: total; *right*: HIPPARCOS. The lower panels show *(left)* $P(p)$ (d) (total), and *right* $P(p)$ (d) HIPPARCOS.

Table 5. Some of the main components in the light-variability of HD 33579. (Only components are listed for which the chance probability of occurrence is < 0.1). Components for which the chance probability is between 0.01 and 0.1 are given by square brackets. The power, in arbitrary units, is given between brackets. The frequencies are given in units of 0.001 d^{-1}.

Period of observations (JD - 244000)	ν_1	ν_2	ν_3	ν_4
1650–2100 (vG)	[6.61] (4)	8.015 (10)	-	-
2400–2800 (vG)	7.129 (11)	-	10.097 (10)	-
2800–3600 (vG)	[6.980] (7)	8.766 (11)	-	-
7800–9000 (HIP)	-	[8.045] (10)	[9.511] (8)	[12.21] (8)
total period (1650–9000)	-	8.32 (16)	9.78 (10)	12.49 (7)
average frequency $(0.001\mathrm{d}^{-1})$	6.91	8.28	9.80	12.35
corresponding period (d)	145	121	102	81

the $\tau = \frac{2}{3}$ level as representative for the atmospheric level from where the main light is emitted. From Kurucz's models (Kurucz 1979) in the range of applicability we found

$$\frac{\Delta \log \rho}{\Delta \log g} = +0.94$$

and

$$\frac{\Delta \log \rho}{\Delta T} = -0.90/1000\, K.$$

With $\Delta \log \rho = 2\Delta \log \nu$ one derives for the frequency ν that the observed variations may correspond to the following variations in the photospheric parameters:

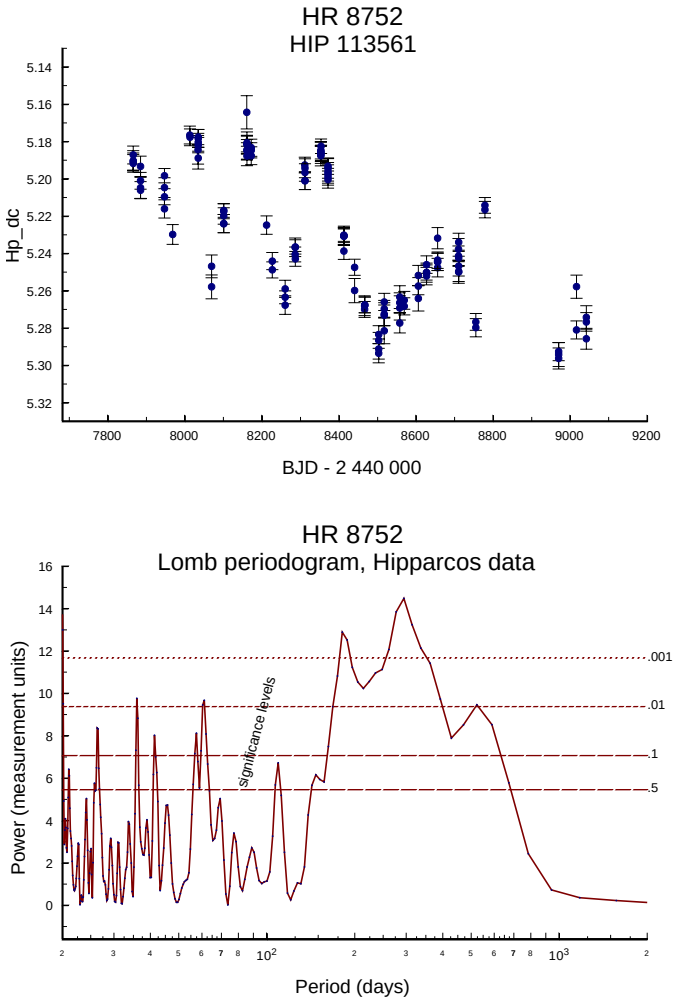

Fig. 5. Light variation of HR 8752. *Upper diagram:* short-time light variations observed by HIPPARCOS. *Lower diagram:* The logarithmic Lomb periodogram as in Fig. 4. The significance levels are for 'false alarm', i.e. low levels of false alarm give high confidence; cf. also Press et al. (1992, pp. 570–571)

– between the first and second period: $\Delta \log g = 0.07$ or $\Delta T_{\rm eff} = -73$ K
– between the second and third period: $\Delta \log g = -0.02$ or $\Delta T_{\rm eff} = +20$ K.

These are very small values, spectroscopically hardly measurable or not at all. We conclude that the observed small variations in the photometric frequencies, if interpreted as described above, offer a way to detect very small variations with time in the photospheric parameters.

6.2. HR 8752

Zsoldos (1986a) finds a secular behaviour, on which is superimposed a periodicity P_q = 400 d (Zsoldos 1986b). Again the HIPPARCOS photometric observations were kindly shown to us by Dr. van Genderen, and are given with their error-bars in the upper panel of Fig. 5. From these data we show a Lomb periodogram in the lower panel of Fig. 5, together with the 'false alarm' significances. Limiting ourselves again to the frequency interval $30 < P < 400$ d, and to chance probabilities < 0.1, we find the periods given in Table 6, together with periods estimated by van Genderen (private communication).

As compared to the fairly 'quiet' star HD 33579 we remark that the number of components is larger in HR 8752. This may be related to its apparent near-instability, in contrast to the former star.

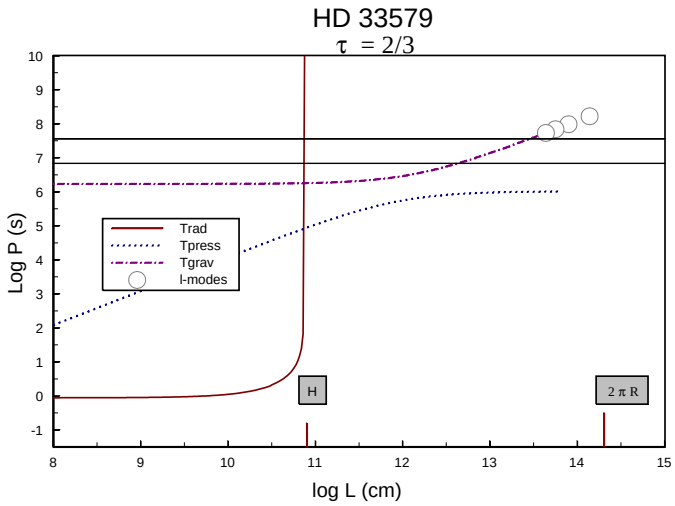

Fig. 6. Diagnostic P, L-diagram of allowed photospheric motions for HD 33579 at τ = 2/3. $T_{\rm rad}$, $T_{\rm press}$ and $T_{\rm grav}$ indicate: gravity waves, pressure (shock) waves and gravity waves respectively. The small lines marked H and $2\pi R$ along the lower part of the diagram indicate the scale height and the stellar circumference. Circles at the right-hand end of the gravity-wave line mark some possible discrete lowest l-number pulsational modes. The two horizontal lines border the region of observed pulsation periods. This should be compared with the allowed modes of pulsation.

Table 6. Basic period P (days) for HR 8752 from long-term photometry (van Genderen, private communication) and from HIPPARCOS data, for false-alarm significance better than 0.1. Periods with a false-alarm signifance between 0.01 and 0.1 are given between square brackets. See Figs. 4 and 5, lower diagrams for more details.

HR 8752	
long term	HIPPARCOS
	510
250	300
190	180
	62
	[58]
	[42]
	37

7. Atmospheric dynamics; (P, L)-diagrams

Our last step is to determine the character of the motions. The allowed motion forms in stellar atmospheres can be studied by means of diagnostic P, L-diagrams, as described by de Jager

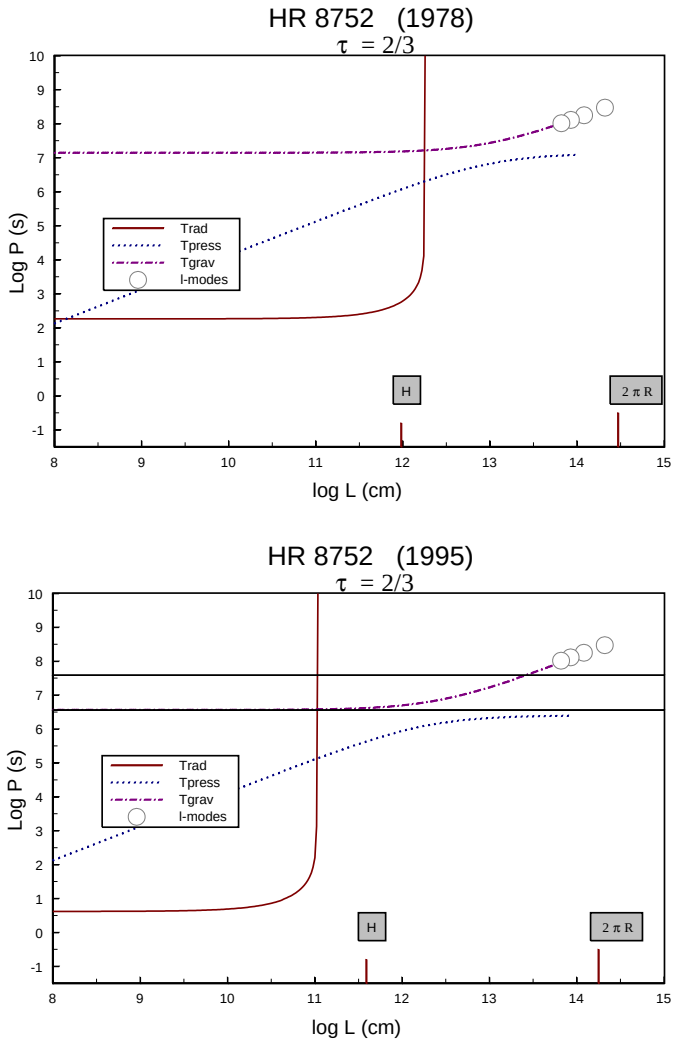

Fig. 7. Diagnostic P, L-diagram of allowed photospheric motions for HR 8752. The diagrams are similar to that of Fig. 6. but now for the observation dates of 1978 and 1995 respectively

et al. (1991) and de Jager (1998). Here, P is the wave-period and L the wavelength. We have derived such diagrams (Figs. 6 and 7) for HD 33579 resp. HR 8752 using the respective data as given in Table 4 from the models that were used to determine the masses. We used photospheric data for the depth level τ = 0.03, considered a representative depth value for line formation. When plotted as done here, the P, L-area where *pressure waves* can occur reduces to a line, drawn as a dotted line in the diagram. It applies to all possible θ-values, where θ is the angle of propagation with respect to the normal. Only in the bending area, where the line approaches the asymptotic value $P_{\rm ac}$, the area broadens somewhat, but to an extent not visible on the scale of the diagram.

The situation is different for *gravity waves*; these can exist in the whole area above the dashed-dotted line. That line corresponds to the case θ = 0 (horizontal propagation). Infinitely long periods correspond to the case $\theta = \pi/2$.

The range of allowed wavelengths is limited since the upper wavelength limit is set by the stellar circumference $2\pi R$. In addition, there is the effect of radiative damping, and layer curvature. The combined effect of damping and curvature is shown by the solid lines in Figs. 6 and 7. These gives for any L-value the time P in which gravity waves are damped in an e-folding time equal to P. Above and to the left of that curve they are damped more rapidly. In the curve for the gravity waves the longest possible discrete periods are shown by the circles at the long-wavelength end of the full-drawn curve. These periods represent low surface l-modes for n = 1, according to $P{\sim}(l(l+1))^{-1/2}$ (Vandakurov 1968; Smeyers & Tassoul 1987).

To facilitate a comparison of these predictions with the observed periods of variability and thus to identify the character of the atmospheric wave motions, we have drawn two horizontal thin lines in the diagrams. These lines limit the area of observed P-values given in Tables 5 and 6.

For HD 33579 (Fig. 6) the conclusion is that the observed variations are due to gravity-wave pulsations with l-values between ≈ 4 and ≈ 20. There is no indication of the existence of p-waves, but that is not surprising since p-waves should have periods shorter than about a week. Existing sets of observations, including the HIPPARCOS data are mostly made with longer time intervals between consecutive observations.

For HR 8752 it is, first of all, important to use the appropriate photospheric model. The HIPPARCOS data refer mainly to the period around 1995, and therefore we used the photospheric data derived for the the observations of April 1995 (Fig. 7, lower panel). Had we used those from 1987 (Fig. 7, upper panel) we would have obtained erroneous results. We find that the observed variations are due to high-l gravity-waves.

8. Conclusions

The conclusions refer to the evolutionary status of the three stars and the dynamical state of their atmospheres.

We confirm the assumption that HR33579 is a slightly evolved star with still a high mass on its redward track in the HR diagram. Hence, its position *inside* the yellow evolutionary void does not conflict with the assumption that stellar atmospheres are unstable inside the void. It pulsates in a restricted number of high l-mode gravity waves.

In contrast, HR 8752 is an evolved star that appears to be near-unstable, as appears from its low mass, its temperature-variations, its regularly occurring periods of mass-loss, which we describe as 'bouncing to the low-T border of the yellow evolutionary void'. Two such bouncings have been identified in the years since 1970. A next mass ejection seems imminent.

Very similar to HR 8752, but studied in less detail, is IRC +10420. This star too appears to be a very evolved star of low mass, that is approaching the void from the red side of the HR diagram while periodically losing mass.

The photometric variations of the stars are due to gravity waves. In HD 33579 these are waves of average l-number, while in HR 8752 the number of components is large while also the l-values of the various components is also large. It may be,

but it is not certain that this difference is related to the stellar (in)stability.

Acknowledgements. We are obliged to the late Dr. Hans Günther Groth for the spectra of HD 33579 he kindly put at our disposal, to the late Dr. Jan Smolinski for his ever ready interest in the status of HR 8752, and for his contribution of spectra taken at Victoria, to M. R. Schmidt for providing us with the equivalent widths and error estimates of one of the spectra provided by J. Smolinski, Dr. René Rutten for the La Palma spectrum of HR 8752 used in this paper, and Dr Alex Lobel for the first reduction of the La Palma spectrum and for his continuing support. Many thanks are due to Dr Arnout van Genderen for his information of long-time photometry of HD 33579 and of HR 8752, including the HIPPARCOS data for these stars before they were published.

Appendix

The various columns in Tables A2 through A5 list: (1) the wavelength in nm; (2) the element and ionization code (e.g. 2600 or 2601 means FeI or FeII); (3) the values of $\log gf$, taken from Martin et al. (1988) and Kurucz & Peytremann (1975); (4) a code indicating the expected accuracy of the $\log gf$-values (cf. Table A1); (5) the measured equivalent widths $W_{\rm obs}$ in nm; (6) the tolerance in $W_{\rm obs}$ in pm, as derived from multiple measured values, or estimated if the number of input data was too small, with an additional estimated term for systematic errors (mainly due to uncertainties in the choice of the level of the continuous spectrum).

The code in the fourth column are indications for the expected accuracy of the $\log gf$-values. We have tentatively transformed them into numerical values. Table A1 lists the adopted logarithmic uncertainty of the values of $\ln gf$ used in this paper.

.1. Spectroscopic stellar data

HD 33579. The spectra studied by us were taken by the late Dr. Hans Günther Groth. The spectra were taken in December 1986 and November 1987 with CASPEC on the ESO 3.6-meter telescope (cf. Humphreys et al. 1991). Copies of the recordings were kindly sent by Dr. Groth to the authors, along with the line identifications.

The equivalent widths $W_{\rm obs}$ were measured from the recordings; for all lines we got several $W_{\rm obs}$-values, hence an average could be taken, and this procedure also provided an indication of the accuracy of the measurements, however not including systematic errors.

HR 8752. We reanalysed spectral data by Luck (1975) obtained in August 1973, by Piters et al. (1988) in July 1984, For the data corresponding to these dates we refer to the original publications. In order to process the data in the same way as the other data we made an estimate of the errors in the observed equivalent widths and added an accuracy code.

HR 8752 spectrum on plate no 12380 has been obtained on 1 August 1978 by J. Smolinski with the coudé mosaic-grating spectrograph at the Dominion Astrophysical Observatory in Victoria, B.C. Canada with a resolution of $\approx$ 42000

Table A1. Adopted numerical values for the uncertainty parameters of the values of $\ln gf$ as given by Martin et al. (1988). The X-parameter was introduced by us as an estimated uncertainty in the Kurucz & Peytremann (1975) gf-values.

symbol	$\Delta \ln gf$
B^+	0.15
C	0.25
C^+	0.30
D^-	0.40
D	0.50
X	0.50

Table A2. Data for HD 33579, see paper for details

λ (nm)	atom	$\log gf$	code	$W_{\rm obs}$	ΔW
397.416	2601	-3.51	D	16.4	2.7
401.240	2201	-1.61	C	31.2	5.5
402.836	2201	-1.00	D	19.2	4.5
412.264	2601	-3.38	D	22.1	3.5
414.387	2600	-0.45	C+	7.8	4.5
418.779	2600	-0.55	B+	5.0	1.7
420.203	2600	-0.71	B+	7.9	3.3
423.881	2600	-0.28	C+	2.7	2.5
425.012	2600	-0.40	B+	5.2	3.1
425.262	2401	-2.39	X	10.0	1.5
425.816	2601	-3.40	D	12.3	3.7
426.928	2401	-2.54	X	6.0	3.5
427.557	2401	-2.12	X	13.8	1.5
427.812	2601	-3.89	X	8.0	1.7
428.240	2600	-0.81	C+	3.7	2.1
428.421	2401	-2.25	X	12.8	3.5
428.788	2201	-2.02	D-	16.5	3.5
429.022	2201	-1.12	D-	40.2	3.3
429.409	2201	-1.11	D-	35.0	5.1
429.657	2601	-3.01	D	23.0	1.3
430.006	2201	-0.77	D-	48.4	2.1
432.096	2201	-1.87	D-	23.1	1.7
432.576	2600	-0.01	C+	17.9	5.1
439.979	2201	-1.27	D-	30.0	2.3
444.378	2201	-0.70	D-	48.9	5.9
446.852	2201	-0.60	D-	49.2	2.5
449.140	2601	-2.70	C	28.0	5.1
450.127	2201	-0.75	D-	43.7	2.5
450.828	2601	-2.21	D	44.8	11.9
451.534	2601	-2.48	D	39.3	6.7
453.961	2401	-2.53	D	3.7	1.3
454.152	2601	-3.05	D	22.9	2.5
456.377	2201	-0.96	D-	46.3	2.5
456.577	2401	-2.11	D	6.8	1.9
456.831	2201	-2.65	D	2.7	1.5
457.633	2601	-3.04	D	21.2	2.7
458.822	2401	-0.63	D	37.2	13.5
459.207	2401	-1.22	D	19.0	1.3
461.664	2401	-1.29	D	13.1	1.7
461.882	2401	-1.11	D	28.7	2.5
462.934	2601	-2.37	D	47.8	1.7
465.697	2601	-3.63	E	10.2	2.5
473.144	2601	-3.36	D	16.1	4.1
480.509	2201	-1.10	D-	14.1	3.9

Table A2. (continued)

λ (nm)	atom	loggf	code	$W_{\rm obs}$	ΔW
481.234	2401	-1.80	D	3.4	2.9
482.412	2401	-1.22	D	26.6	2.1
484.824	2401	-1.14	D	23.1	2.5
485.618	2401	-2.26	D	4.5	3.1
486.432	2401	-1.66	X	21.8	2.5
487.401	2201	-0.79	D	8.9	4.9
487.641	2401	-1.46	D	30.6	7.5
491.118	2201	-0.34	D	8.5	2.5
509.733	2401	-2.64	D	2.4	1.9
510.066	2601	-4.37	D	4.7	1.5
516.082	2601	-2.82	X	3.8	1.5
518.590	2201	-1.35	D	7.0	1.5
519.494	2600	-2.09	B+	0.9	1.3
519.756	2601	-2.10	C	38.9	1.9
523.462	2601	-2.05	C	35.4	2.5

Table A3. Data for HD 33579, continued

λ (nm)	atom	loggf	code	$W_{\rm obs}$	ΔW
523.735	2401	-1.16	D	18.3	1.9
526.481	2601	-3.19	D	8.0	2.3
527.600	2601	-1.94	C	41.0	4.9
531.361	2401	-1.65	D	5.6	3.3
531.662	2601	-1.85	C	51.8	3.7
536.286	2601	-2.92	X	25.3	9.7
542.526	2601	-3.54	X	7.2	2.1
553.483	2601	-2.93	D	13.2	4.5

Table A4. Data for HR 8752 (1978/08): as Table A2, further: below the middle line the data give results that lead to differences in equivalent width that are $> 3.5\sigma$ from the expected values. Spectra taken by J. Smolinski. Equivalent widths derived by M.R. Schmidt.

λ (nm)	atom	loggf	code	$W_{\rm obs}$	ΔW
487.132,	2600,	-0.41,	C+,	67.4,	6.7
489.382,	2601,	-4.45,	D,	42.1,	4.2
490.332,	2600,	-1.08,	C,	42.2,	4.2
491.900,	2600,	-0.37,	C+,	66.8,	3.3
496.610,	2600,	-0.89,	C+,	33.1,	3.3
501.208,	2600,	-2.64,	B+,	68.4,	6.8
504.983,	2600,	-1.42,	C,	57.6,	2.9
505.164,	2600,	-2.80,	B+,	58.0,	2.9
513.370,	2600,	0.14,	D,	41.9,	4.2
516.118,	2601,	-4.77,	X,	45.4,	11.4
516.228,	2600,	0.02,	D,	43.0,	8.6
520.235,	2600,	-1.84,	B+,	41.9,	4.2
522.986,	2600,	-0.91,	X,	27.1,	8.1
523.463,	2601,	-2.05,	C,	100.5,	10.1
526.656,	2600,	-0.49,	C+,	57.3,	2.9
528.180,	2600,	-1.02,	C,	33.2,	1.7
530.231,	2600,	-0.88,	C+,	48.5,	2.4
531.662,	2601,	-1.85,	C,	98.1,	24.5
532.419,	2600,	-0.24,	C+,	56.5,	2.8
532.556,	2601,	-2.60,	C,	53.4,	2.7
536.748,	2600,	0.35,	C+,	33.4,	1.7
537.150,	2600,	-1.64,	B+,	88.3,	8.8

Table A4. (continued)

λ (nm)	atom	loggf	code	$W_{\rm obs}$	ΔW
537.914,	2600,	-1.99,	B+,	87.6,	8.8
538.338,	2600,	0.50,	C+,	42.3,	2.1
538.946,	2600,	-0.41,	D-,	16.5,	1.7
540.051,	2600,	-0.16,	D,	24.8,	2.5
540.414,	2600,	0.02,	X,	52.3,	20.9
540.578,	2600,	-1.84,	B+,	75.1,	7.5
542.408,	2600,	0.52,	D,	60.8,	6.1
542.526,	2601,	-3.36,	D,	42.1,	4.2
542.970,	2600,	-1.88,	B+,	78.8,	7.9
543.453,	2600,	-2.12,	B+,	65.0,	5.2
544.505,	2600,	-0.02,	D,	26.0,	2.6
545.562,	2600,	-2.00,	X,	68.1,	17.0
549.752,	2600,	-2.85,	B+,	57.1,	14.3
550.678,	2600,	-2.80,	B+,	44.8,	2.2
556.963,	2600,	-0.54,	C+,	37.8,	1.9
557.285,	2600,	-0.31,	C+,	38.9,	3.9
557.610,	2600,	-1.00,	C,	30.8,	1.5
558.677,	2600,	-0.21,	C+,	53.8,	2.7
561.563,	2600,	-0.14,	C+,	51.1,	5.1
562.456,	2600,	-0.90,	C+,	30.0,	3.0
568.653,	2600,	-0.63,	C,	15.1,	6.0
586.237,	2600,	-0.60,	X,	11.4,	5.7
492.393,	2601,	-1.32,	C,	137.6,	6.9
501.845,	2601,	-1.22,	C,	159.4,	23.9
515.192,	2600,	-3.32,	B+,	47.1,	4.7
519.758,	2601,	-2.10,	C,	95.7,	4.8
536.287,	2601,	-2.92,	X,	75.4,	3.8
541.408,	2601,	-3.79,	D,	67.4,	6.7

Table A5. Data for HR 8752 (1995/04): as Table A2, further: below the middle line the data give results that lead to differences in equivalent width that are $> 3.5\sigma$ from the expected values. Spectra taken by René Rutten. Equivalent widths derived by A. Lobel and one of the authors (H.N.).

λ (nm)	atom	loggf	acc. symb.	$W_{\rm obs}$	ΔW
449.140,	2601,	-2.70,	C,	59.6,	4.4
450.127,	2201,	-0.75,	D-,	83.0,	1.6
451.534,	2601,	-2.48,	D,	75.8,	4.9
456.578,	2401,	-2.11,	D,	24.7,	2.6
456.831.,	2201,	-2.65,	D,	20.1,	3.8
457.197,	2201,	-0.53,	D-,	81.0,	1.1
457.633,	2601,	-3.04,	D,	52.0,	3.2
459.202,	2401,	-1.22,	D,	41.6,	2.7
465.697,	2601,	-3.63,	E,	44.1,	2.8
473.144,	2601,	-3.36,	D,	47.7,	2.4
480.510,	2201,	-1.10,	D-,	58.4,	2.6
481.235,	2401,	-1.80,	D,	25.6,	1.8
486.432,	2401,	-1.66,	X,	29.9,	2.6
487.402,	2201,	-0.79,	D,	34.1,	3.7
487.641,	2401,	-1.46,	D,	46.8,	4.9
489.382,	2601,	-4.45,	D,	13.6,	5.7
490.332,	2600,	-1.08,	C,	7.6,	5.0
491.120,	2201,	-0.34,	D,	50.2,	5.0
491.900,	2600,	-0.37,	C+,	17.2,	2.7
504.983,	2600,	-1.42,	C,	7.0,	4.4

Table A5. (continued)

λ (nm)	atom	loggf	acc. symb.	$W_{\rm obs}$	ΔW
509.729,	2401,	-2.64,	D,	13.0,	4.7
510.066,	2601,	-4.37,	D,	21.9,	3.6
516.228,	2600,	0.02,	D,	11.8,	4.1
518.590,	2201,	-1.35,	D,	42.0,	3.7
519.758,	2601,	-2.10,	C,	69.4,	3.1
520.235,	2600,	-1.84,	B+,	6.5,	3.1
523.463,	2601,	-2.05,	C,	65.4,	2.7
523.734,	2401,	-1.16,	D,	42.1,	4.2
526.480,	2601,	-3.19,	D,	45.3,	2.6
526.656,	2600,	-0.49,	C+,	13.4,	2.3
528.180,	2600,	-1.02,	C,	8.7,	2.3
530.231,	2600,	-0.88,	C+,	10.0,	2.7
531.361,	2401,	-1.65,	D,	28.4,	2.5
532.419,	2600,	-0.24,	C+,	23.4,	2.2
533.483,	2401,	-1.79,	X,	26.5,	3.5
536.287,	2601,	-2.92,	X,	57.6,	2.1
536.748,	2600,	0.35,	C+,	11.2,	4.1
538.101,	2201,	-2.08,	D,	32.5,	5.1
538.338,	2600,	0.50,	C+,	13.1,	4.5
541.876,	2201,	-2.07,	X,	25.0,	4.2
542.091,	2401,	-2.36,	D,	12.9,	4.9
542.408,	2600,	0.52,	D,	15.3,	3.3
542.526,	2601,	-3.36,	D,	32.1,	3.8
543.256,	2500,	-3.80,	C+,	20.6,	2.5
544.505,	2600,	-0.02,	D,	8.0,	3.2
550.863,	2401,	-2.11,	D,	12.7,	2.6
552.679,	2101,	0.13,	D,	53.3,	2.8
553.483,	2601,	-2.93,	D,	46.8,	4.3
559.374,	2800,	-0.84,	D-,	9.8,	5.1
561.563,	2600,	-0.14,	C+,	20.7,	4.6
608.410,	2601,	-3.98,	D,	14.7,	3.8
611.333,	2601,	-4.31,	D,	9.8,	3.9
614.925,	2601,	-2.92,	D,	36.7,	7.0
624.632,	2600,	-0.96,	D-,	24.3,	3.4
624.755,	2601,	-2.51,	D,	46.7,	4.8
641.692,	2601,	-2.92,	D,	23.4,	3.0

(from Fletcher et al. 1980). The heliocentric velocity correction registered on the original plate is $Vr_{\rm sun}$ = +15.84 km s^{-1}. The spectrum was reduced by M. R. Schmidt, who kindly provided us with the list of equivalent widths, presented here.

The 1995 spectrum was taken with the courtesy of Dr. René Rutten with the Utrecht Echelle Spectrograph at La Palma with a resolution of about 80000 and was reduced by A. Lobel together with one of the authors (H. N.). The equivalent widths are published here.

IRC +10420. We used the spectral line data given in Appendix A of Oudmaijer (1995), taken on 26/27 and 27/28 July 1994 at La Palma, Spain, with a resolution of $\approx$ 30.000. An estimation was made of errors in the observed equivalent widths and an accuracy code was added. The lines were screened for unblended single lines and the hydrogen (and telluric) lines were excluded.

References

Achmad L., de Jager C., Nieuwenhuijzen H., 1991a, A&A 249, 292
Achmad L., de Jager C., Nieuwenhuijzen H., 1991b, A&A 250, 445
Baschek Z., Holweger H., Traving G., 1966, Abhandl. aus der Hamburger Sternwarte, Band VIII, Nr 1 p. 26
Burger M., 1976, Thesis, Vrije Universiteit Brussel, Brussel
de Jager C., 1980, The Brightest Stars, Reidel, Dordrecht
de Jager C., 1998, A&AR 8, 39
de Jager C., Nieuwenhuijzen H., 1987, A&A 177, 217
de Jager C., Nieuwenhuijzen H., 1997, MNRAS 290, L50
de Jager C., Nieuwenhuijzen H., van der Hucht K.A., 1988, A&AS 72, 259
de Jager C., de Koter A., Carpay J., Nieuwenhuijzen H., 1991, A&A 244, 131
de Jager C., Lobel A., Israelian G., 1997, A&A 325, 714
Fletcher J.M., Harmer C.F.W., Harmer D.L., 1980, The Instrumental Profile of a Mosaic-grating Spectrograph, Publ. Dominion Astrophysical Observatory, Victoria, B.C. Vol. XV, No. 11
Fry M.A., Aller L.H., 1975, ApJS 29, 55
Grieve G.R., Madore B.F., 1986a, ApJS 62, 427
Grieve G.R., Madore B.F., 1986b, ApJS 62, 451
Groth H.G., Kudritzki R.P., Butler K., Humphreys R.M., 1992, in Heber U., Jeffery C.S. (eds.), The Atmospheres of Early-Type Stars, Lecture Notes in Physics 401, Springer Verlag, Berlin, p. 53
Humphreys R.M., 1989, in Davidson K., Moffat A.F.J., Lamers H.J.G.L.M. (eds.), Physics of Luminous Blue Variables, Kluwer, Dordrecht, p3
Humphreys R.M., Davidson K., 1979, ApJ 232, 409
Humphreys R.M., Strecker D.W., Murdock T.L., Low F.J., 1973, ApJ 179, L49
Humphreys R.M., Kudritzki R.P., Groth H.G., 1991, A&A 245, 593
Humphreys R.M., Smith N., Davidson K., et al., 1997, AJ 114, 2778
Iriarte B., Johnson H.L., 1965, Sky & Tel 30, 21
Johnson H.L., Morgan W.W., 1953, ApJ 117, 313
Keenan P.C., 1971 Contr. Kitt Peak Natl. Obs. 554, 35
Klochkova V.G., Chentsov E.L., Panchuk V.E., 1997, MNRAS 292, 19
Kraft R.P., Hiltner W.A., 1961, ApJ 134, 850
Kurucz R.L., 1979, ApJS 40,1
Kurucz R.L., Peytremann E., 1975, A table of semi-empirical gf values, Special Report 362, Smithsonian Astrophys. Obs., Cambridge, Mass.
Lambert D.L., Luck R.E., 1978, MNRAS 184, 405
Lambert D.L., Hinkle K.H., Hall D.N.B., 1981, ApJ 248, 638
Lobel A., Achmad L., de Jager C., Nieuwenhuijzen H., 1992, A&A 256, 159
Lobel A., Israelian G., de Jager C., et al., 1998, A&A 330, 659
Luck R.E., 1975, ApJ 202, 743
Maeder A., Meynet G, 1987, A&A 182, 243
Maeder A., Meynet G., 1988, A&AS 76, 411
Martin G.A., Fuhr J.R., Wiese W.L., 1988, J. Phys Chem Ref Data 17, Suppl. nrs. 3 and 4
Morgan W.W., Keenan P.C., Abt H.A., Tapscott J.W., 1981, ApJ 243, 894
Nieuwenhuijzen H., de Jager C., 1990, A&A 231, 134
Nieuwenhuijzen H., de Jager C., 1995a, A&A 302, 811
Nieuwenhuijzen H., de Jager C., 1995b, in Noels A., Fraipont-Caro F., Gabriel M., Grevesse N., Demarque P. (eds.), Stellar Evolution; What Should be Done, Liege Univ., p. 239
Oja T., 1963, Ark. Astron. 3, 273
Oudmaijer R.D., 1995, Thesis, Groningen
Oudmaijer R.D., 1998, A&AS 129, 541

Oudmaijer R.D., Groenewegen M.A.T., Matthews H.E., Blommaert J.A.D.L., Sahu K.C., 1996, MNRAS 280, 1062
Patterson R.S., 1990, AJ 99, 1953
Percy J.R., Zsoldos E., 1992, A&A 263, 123
Piters A., de Jager C., Nieuwenhuijzen H., 1988, A&A 196, 115
Press W.H., Teukolsky S.A., Vetterling W.T., Flannery B.P., 1992, Numerical Recipes in Fortran, The Art of Scientific Computing, 2nd edition, Cambridge University Press, New York
Przybylski A., 1968, MNRAS 139, 313
Sandage A., Smith L.L., 1963, ApJ 137, 1057
Sargent W.L.W., 1965, the Obs. 85, 33
Sheffer Y., Lambert D.L., 1987, PASP 99, 1277
Sheffer Y., Lambert D.L., 1992, PASP 104, 1054
Smeyers P., Tassoul M., 1987, ApJS 65, 429
Smith K.C., Howard I.D., 1998, MNRAS 299, 1146
Smolinski J., Climenhaga J.L., Fletcher J.M., 1989, in Davidson K., Moffat A.F.J., Lamers H.J.G.L.M. (eds.), Physics of Luminous Blue Variables, Kluwer, Dordrecht, p. 131
Stahl O., Aab O., Smolinski J., Wolf B., 1991, A&A 252, 693
Tifft W.G., Snel Ch.M., 1971, MNRAS 151, 365
Vandakurov Yu. V., 1968, Sov. Astron. 23, 421
van Genderen A., 1979a, A&AS 38, 151
van Genderen A., 1979b, A&AS 38, 381
van Leeuwen F., van Genderen A.M., Zegelaar I., 1998, A&AS 128, 117
Walker A.R., 1999 in Heck A., Caputo F. (eds.), Post Hipparcos Cosmic Candles, Astroph. and Space Science Lib. vol. 237, Kluwer Academic Publishers, Dordrecht, p. 140
Walraven Th., Walraven J., 1971, in Muller A.B. (ed.), The Magellanic Clouds, Reidel Publ. Co., Dordrecht, Holland, p. 117
Wares G.W., Ross J.E., Aller L.H., 1968, Ap&SS 2, 344
Wolf B., 1972, A&A 20, 285
Zsoldos E., 1986a, the Obs. 106, 156
Zsoldos E., 1986b, in de Loore C.W.H., Willis A.J., Laskarides P. (eds.), Luminous Stars and Associations in Galaxies, I.A.U. Symp. No. 116, Reidel Publ. Co., Dordrecht, p. 87